AIAA AVIATION Forum
12-16 June 2023, San Diego, CA and Online
AIAA AVIATION 2023 Forum

Microstructure Controlled Multi-Layer Porous Material Liner Tested On The Advanced Noise Control Fan

Bharath Kenchappa[1] and Kunigal Shivakumar[2]
North Carolina A&T State University, Greensboro, NC, 27411, USA

Daniel Sutliff[3]
NASA Glenn Research Center, Cleveland, Ohio, 44135, USA

A novel concept of multilayer micro structurally controlled noise mitigation porous material was developed and experimentally validated in the laboratory by normal incidence impedance test. Extensive parametric studies were made to understand various parameters that influence acoustic absorption and transmission loss based on the test specimen size, particle size, porosity, pore size, and its distribution through the thickness. The results were reported in many publications. This work was focused on applying the concept and assessing the validity of the technology to aircraft turbomachine engines. The NASA Glenn Research Center's Advanced Noise Control Fan (ANCF) low-speed test rig was selected. The liner insert required a 4-ft internal diameter cylinder with a 2-inch thick and 9-inch axial length. The liner was fabricated in eight segments and assembled in an aluminum test rig. The liner was tested for both tonal and broadband noise at the Notre Dame Turbomachinery Lab White Field test facility, where the ANCF is located. The study concludes that: Microstructurally controlled porous material is very effective in dissipating the sound energy; the liner is effective for tonal noise (2 to 13 dB reduction in noise levels) that constitutes the major part of the overall fan noise, especially the blade passing frequency which is generally the dominating component; Also, the liner is effective for broadband noise with reductions in sound pressure level of about 3 dB for the shaft order greater than 20. The proposed two-layer liner model demonstrated the validity of the concept. More studies are required to optimize the design.

I. Nomenclature

BPF	=	Blade passing frequency
d_m	=	Mean particle diameter
D_i	=	Inner diameter
D_o	=	Outer diameter
l	=	Axial length
t	=	Specimen thickness
ANCF	=	Advanced noise control fan
SPL	=	Sound pressure level
dB loss	=	Loss in decibels
α	=	Sound absorption coefficient
TLn	=	Transmission Loss
RPM	=	Revolutions per minute

[1] Research Associate, Center for Composite Materials Research, Department of Mechanical Engineering.
[2] Research Professor and Director, Center for Composite Materials Research, Department of Mechanical Engineering, Associate Fellow AIAA, Member ASME
[3] Experimental Acoustics Researcher, NASA Glenn Research Center, Associate Fellow AIAA

II. Introduction

A novel concept of multilayer micro structurally controlled noise mitigation porous material was developed and experimentally validated in the laboratory by normal incidence impedance test and detailed in the reference [1]. Porous sound absorption materials have gained interest in the field of noise mitigation as they are composed of channels, cracks, or cavities which allow the sound waves to enter the materials. Sound energy is dissipated by thermal loss caused by the friction of air molecules with the pore walls, and vicious loss brought by the viscosity of airflow within the materials. These energy consumption principles endow porous materials with a broad frequency band for sound absorption [2, 3]. They are usually cellular, fibrous, or granular, this classification is based on the microscopic structure [4, 5]. Among these types of material systems, we focused on microstructure-controlled granular porous materials as they allow designing porous sound absorbers of engineered acoustic response by controlling the porosity, pore size and their distribution through the thickness by appropriate selection of particles and the surface imperfections of the particles improves fluid flow resistance and tortuosity. Natural granular ceramic hollow microbubbles commercially available and supplied by Sphere One – called Extendospheres that are the byproducts of coal-burned electric power plants were selected. These are lightweight ceramic particles filled with air characterized by size. Also, this material can be multifunctional by offering thermal management. A new particle surface coating technique with a minimal polymer binder was developed to mimic the pore properties of the loose granular system to maintain near-similar porosities. The processing and fabrication of this new material system addressed as micro-porous hollow bubble (μPHB) composite material is described in detail in reference [6]. An extensive experimental and analytical study was conducted on single-layer specimens in terms of particle diameter, pore size and their distribution, and specimen thickness [1]. Several different particle size single layer specimens of 100 mm diameter, 25 and 50 mm thick were fabricated and impedance tested. Firstly, the particle size must be less than 1 mm to achieve effective acoustic responses was demonstrated [1]. Then we concluded that for a given frequency, the absorption is higher for larger-size particles and alternatively, it is lower for smaller-size particles. Transmission (sound energy) loss directly increased with a decrease in pore size (particle size) and with the increase in specimen thickness. The two extreme responses from the single-layer materials lead to the conclusion that both high sound absorption and transmission loss cannot be achieved by single-size particle distribution through the thickness. An alternative approach of different size particle distribution, in other words, a multilayer approach using different size particles is needed. This was demonstrated both by experimentation and analyses in the reference [1]. A three-layer model (layers of different thicknesses but with a total thickness of 50 mm), with graded distribution from large to small particle size; led to an absorption coefficient (α) > 0.70 and transmission loss (TLn) > 20 dB in the transportation noise frequency range of 800 to 1,200 Hz and beyond 1,200 Hz the α remained constant and TLn increased with frequency. In the normal incidence case, the concept of material development was demonstrated but a liner in the case of duct or grazing flow inside an aircraft engine was to be tested and validated.

The objective of this work is to validate the microstructurally controlled multilayer material for a turbomachine engine. The NASA Glenn Research Center's Advanced Noise Control Fan (ANCF) low-speed test rig [7] was chosen. The liner specs include an inner diameter of 48″, an outer diameter of 52″, a length of 9″, and a liner thickness of 2″. We chose a two-layer material system with each layer of 1-inch thickness; the innermost layer was made of large-size particles with a mean particle diameter of 625 μm and the outer layer was made of medium-sized particles with a mean particle diameter of 160 μm. The liner was tested at the Notre Dame Turbomachinery Lab Whitefield [8] test facility. The dB loss from this two-layer graded porous material liner relative to baseline configuration was determined to assess the impact of the proposed concept.

III. Laboratory Test

A two-layer graded porous material cylindrical specimen of 100 mm diameter and 50 mm total thickness (each layer 25 mm thick) was fabricated, and normal incidence impedance was tested to measure absorption coefficient versus frequency using two microphone setup according to ASTM E1050-12 [9] standard and transmission loss versus frequency using four-microphone setup according to ASTM 2611-09 standard [10]. All the test details and smoothening of the raw data are provided in reference [6]. Fig 1. shows the absorption coefficient versus frequency and from the result, we see that the absorption coefficient is > 0.50 beyond 600 Hz, then reaches a maximum value of 0.75 @ 1,000 Hz and remains constant throughout the specified frequency range. Fig 2. Shows the transmission loss versus frequency and from the result the transmission loss is > 20 dB beyond 600 Hz and increases with frequency in the specified frequency range. These test results were slightly lower than the three-layer model results [1].

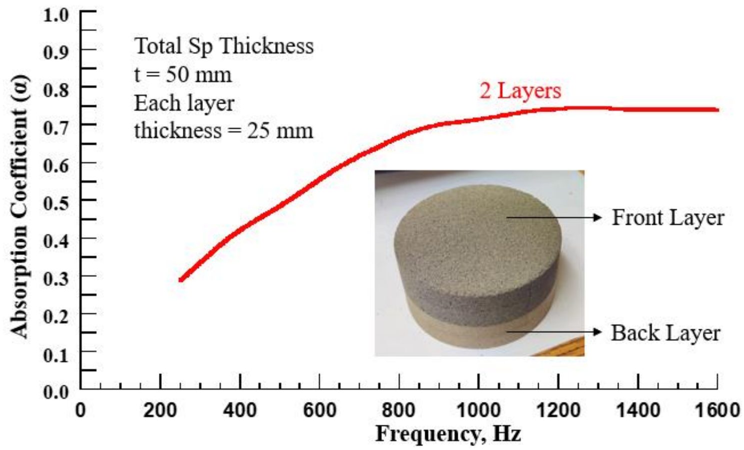

Fig. 1 Absorption coefficient versus frequency response for a two-layer μPHB composite material

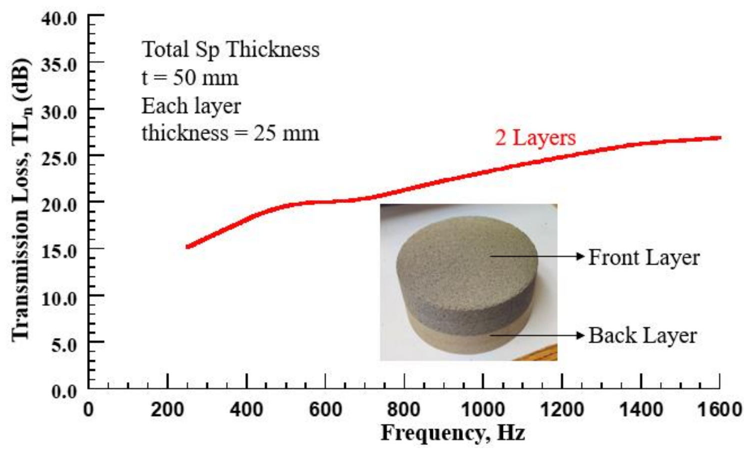

Fig. 2 Transmission loss versus frequency response for a two-layer μPHB composite material

IV. Design of the Mold

The liner is envisioned to be made of eight 45º segments. The mold is made of aluminum for ease of handling. Therefore, an aluminum mold of (see Fig 3) 45º segment with inner diameter D_i = 48″, outer diameter, D_o = 52″, thickness t = 2″ (50 mm), and axial length l = 9″ was designed and fabricated. The mold was fabricated by the local industry. The mold was tested to validate the geometry. This represents one of the eight segments that go around the liner cavity.

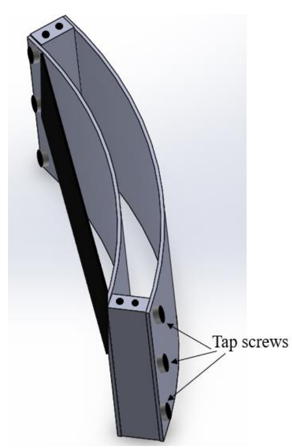

Fig. 3 Aluminum mold of one segment

V. Fabrication of a Liner Segment

The liner segments of 45º each were fabricated in 8 segments to form a full liner. The fabrication of a liner segment consists of 7 steps as shown in Fig. 4. Each of these steps is described below.

Step 1

The required amount of particles of large and medium size was surface coated with SC1008 and prepared before the fabrication. The mold setup is shown in Step 1 of Fig. 4. Tap screws were used for the mold assembly and were only finger-tightened before fabrication. A steel grid of open area fraction of 55% and a wire diameter of 0.016″ was used as a separator for two layers. Two ash composite supports each of ≈1″ thickness were placed at five locations to hold the steel grid in place during the fabrication process. These supports split the mold cavity into four parts marked (a), (b), (c), and (d) as shown in step 3 of Fig 4.

Step 2

Each split cavity on the outer diameter portion was filled with medium size resin coated particles to 1/4th of the height of the liner segment, then the inner diameter portion of the liner segment was filled with large size resin coated particles to 1/4th of the height of the liner segment as shown in step 2 of Fig 4.

Step 3

Once all four split cavities were filled with the particles (Extendospheres), a wooden rod of ≈1″ diameter was used to ram the material. First, the medium-sized particles were rammed starting from cavity (a) as shown in step 3 of Fig 4, followed by cavities (b), (c), and (d). Next, the large-size particles were rammed in the same order.
Step 2 was repeated followed by step 3, then the ash composite supports were removed one after the other from all five locations. Filled additional material at the locations where the ash composite supports were placed using a small scoop, then made sure there is material continuity in both layers.

Step 4

An aluminum ram of 44º segment was used to ram the entire cavity as shown in Step 4. The same order of ramming i.e., the medium size first and then the large size particles was followed.

Step 5

After ramming manually, the aluminum ram was hit with the hammer to achieve good compaction. A partially filled cavity with two layers of medium and large-size particles separated by the steel grid is shown in Fig 4. The mold was filled with the material again and step 4 was repeated. This process of filling the material and repeating step 4 continued until the mold cavity was filled.

Step 6

The mold was covered using the top aluminum plate, compacted the material using the hammer by hitting the top plate, and bolted. Tightened all the tap screws which were finger-tightened initially. Further three C clamps were attached and tightened as shown in Step 6 to avoid lateral expansion during the curing process.

Step 7

The mold was then kept inside the oven for curing. The curing steps were the same as specified in the reference [6].

8 two-layer liner segments of 45º each with inner diameter Di = 48″, outer diameter, Do = 52″, thickness t = 2″ (50 mm) and axial length l = 9″ were manufactured following the same processing steps. A fabricated liner segment and fully arranged liner segments are shown in Fig 5 (a) and (b) respectively.

Fig. 4 Fabrication steps of the liner segments

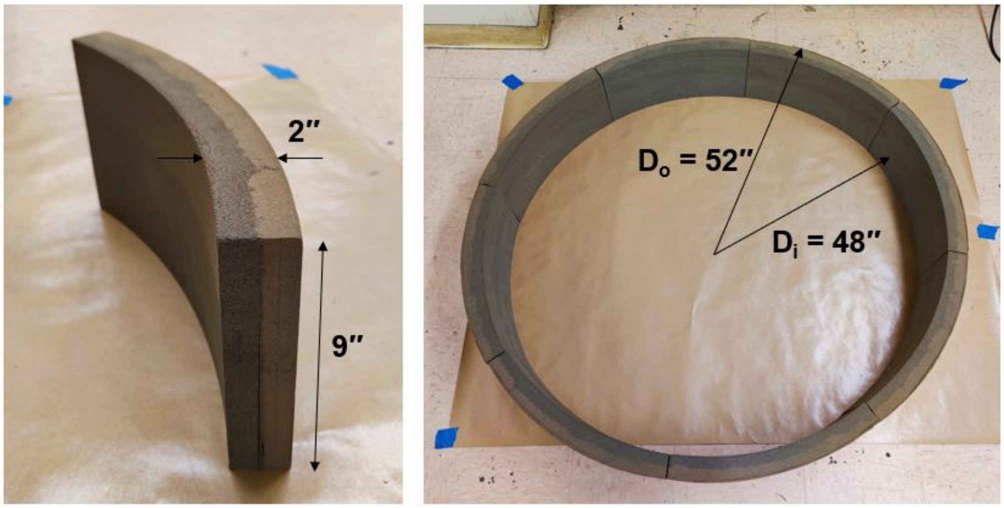

Fig. 5 (a) A two-layer 45^0 segment (b) A full liner arrangement

VI. Acoustic Liner Assembly and Installation

The liner segments were carried to the Notre Dame Turbomachinery Lab for testing.

Firstly, the eight liner segments' height was adjusted to fit the test rig, each segment was slid inside the holder with four liner segments on top and four on the bottom half of the holder as shown in Fig 6 (a). The liner segments were covered with a perforated sheet of open area fraction 0.40 and screwed onto the holder (see Fig 6 (b)). This covering was for surface protection of the liner segments, and it wouldn't alter the performance of the liner (verified before through a normal incidence test). Next, the liner portion of both the top and bottom half of the holders was covered with aluminum tape to acquire baseline test data (see Fig 6 (c)).

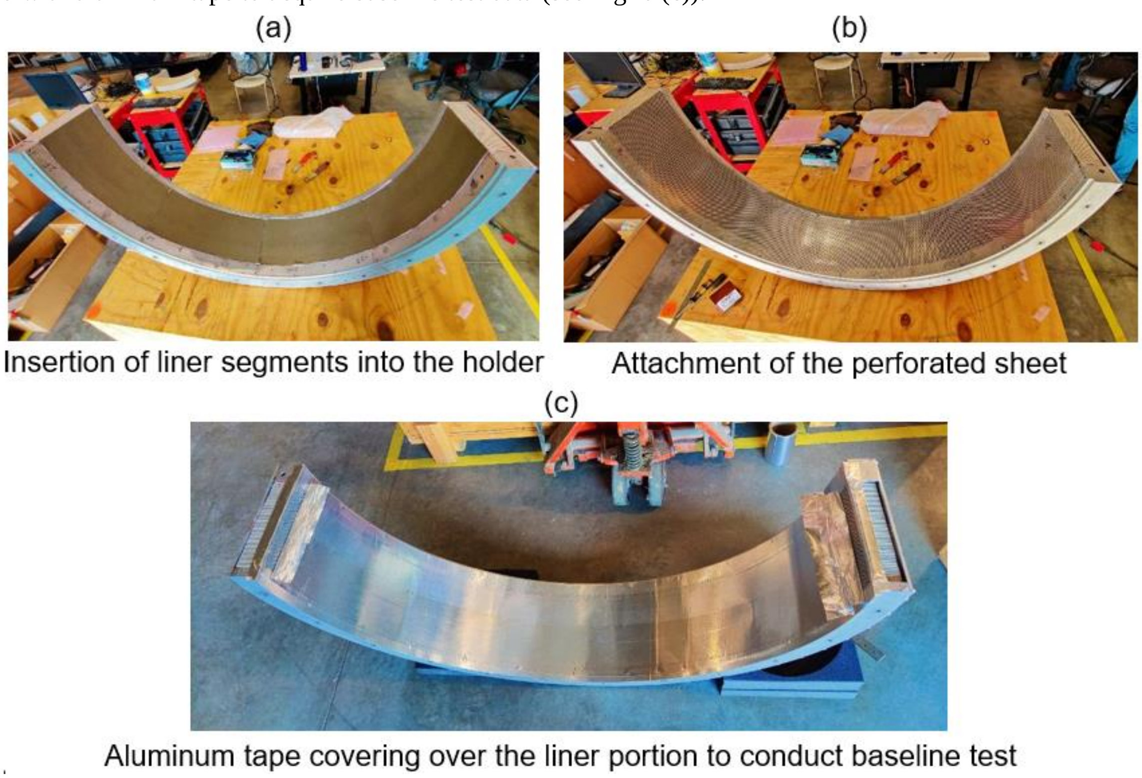

Fig. 6 Liner segment installation inside the test holder

The bottom half of the liner holder was assembled onto the Engine first then the top half of the holder was assembled with the help of the crane as shown in Fig 7.

Fig. 7 Liner installed holder assembly into ANCF test rig

VII. Acoustic Liner Test on NASA GRC's ANCF Engine

The test conditions involved acquiring baseline data (sound pressure level (SPL)) with an aluminum tape on the liner installed inside the liner holder over a corrected fan speed range of 1,500 to 2,000 rpm and were compared with the previous baseline data measurements for repeatability. These measurements were taken in the rotor alone (16 blades @ 28 deg pitch) and with 14 vanes at 1 chord spacing. The same configuration was used to acquire liner data by taking off the aluminum tape. The plan view of the ANCF test rig and the microphones are shown in Fig 8. Far-field acoustic measurements were acquired using 30 microphones placed at a 12-foot radius from the duct centerline and 10 feet high. Fifteen (1-15) of these were in an arc about the inlet exit plane (0° - 90° measured from the inlet axis, Fwd array) and Fifteen (16-30) were in an arc about the exhaust exit plane (90°–160° Aft array with 180° being the exhaust axis). Fig. 9 shows the ANCF test setup with all the microphones arranged to acquire far-field data for baseline and liner configurations.

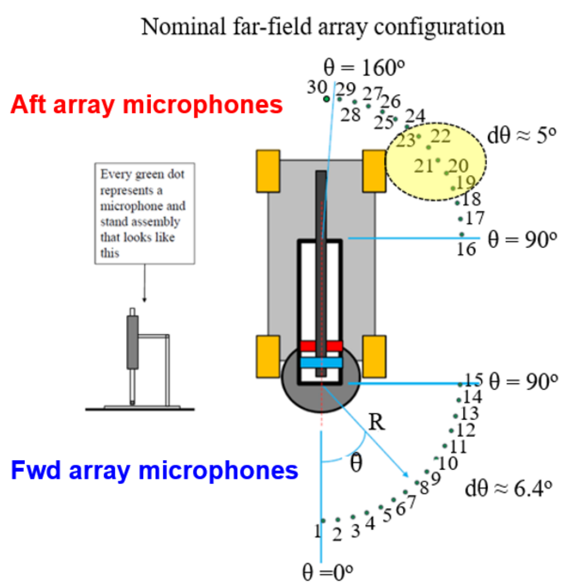

Fig. 8 Plan view of the test setup with ANCF and Microphones

Fig. 9 ANCF test setup to acquire far field data for baseline and liner configurations

VIII. Acoustic Liner Test Results

The time histories were processed using ensemble averaging to analyze the tone and broadband components separately by extracting the tones generated by the fan (shaft orders and harmonics). This can be done exactly since the data are acquired synchronously to the shaft rotation [11]. In this testing, the dynamic test data was recorded and given in the form of Matlab scripts. By running the ANCF code the data was extracted as a spectral file in the Matlab format. The spectral file was run to extract the tone and the broadband sound pressure level (SPL) separately. This process of data extraction was followed for both baseline and liner cases. The shaft speed of the 2,000 RPM test case was chosen for the initial result analyses as this speed is considered the baseline.

A. Effect of Microphone Locations on SPL - Shaft speed of 2,000 RPM

This particular study was carried out to understand how the microphone's location impacts the reduction in the sound pressure level for the liner relative to the baseline. As discussed earlier, Farfield acoustic measurements were acquired using 30 microphones placed at a 12-foot radius from the duct centerline and 10 feet high. Fifteen (1-15) of these were in an arc about the inlet exit plane (0° - 90° measured from the inlet axis, Fwd array) and Fifteen (16-30) were in an arc about the exhaust exit plane (90°–160° Aft array with 180° being the exhaust axis) (see Fig. 8).

1. Forward array microphones

In these microphones 1- 15 which were placed at the inlet exit plane, we noticed that there is insignificant or no difference in SPLs between baseline and liner and this is expected as the microphone locations are at the inlet ahead of the liner setup i.e., before engine sound flow takes place through the duct.

2. Aft array microphones

The aft array microphones (16-30) recorded both tonal and broadband dB loss between the baseline and the liner configuration. The dB loss was maximum in the microphones 19 to 23. This is highlighted in Fig. 8. From the analysis, we noted that the liner was effective beyond the 20-shaft order. For more detailed analysis, we chose a single microphone case i.e., microphone 21 in the region of the maximum reduction in sound pressure level for 2,000 RPM to compare baseline and liner configuration results, understand, smoothen, and analyze the data.

B. Comparison of Test Results between Baseline and Liner Configuration

This section will discuss the test results for tonal and broadband sound pressure levels and dB loss response between the baseline and liner configurations.

1. Tonal sound pressure level response

Fig 10 shows the tonal SPL (dB) versus shaft order for both baseline and liner configuration for microphone 21 for 2,000 RPM. We noticed there are 8xBlade Passing Frequencies (BPF) in addition to tonal noise at other frequencies. From the results, we did notice a reduction in sound pressure level between the baseline and liner beyond the 20 Shaft order.

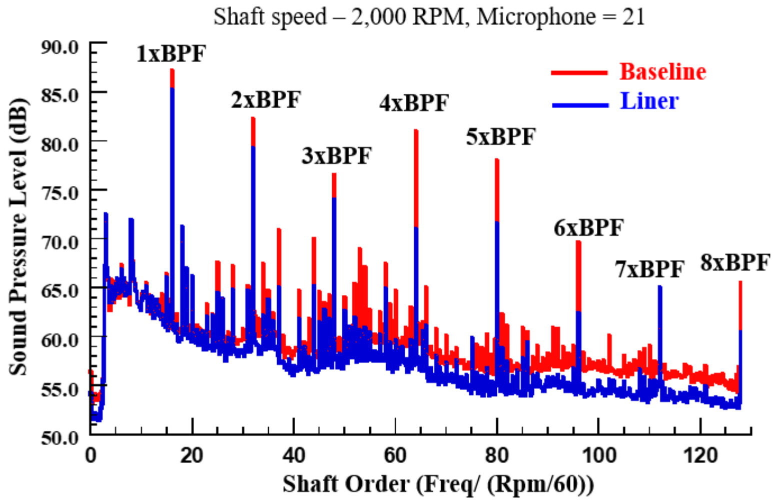

Fig 10. Tonal SPL versus shaft order for baseline and liner configurations

Tonal noise constitutes the major part of the overall fan noise, especially the blade passing frequency which is generally the dominating component. Therefore, a separate tonal BPF response analysis was done to understand and interpret the effectiveness of the liner. Fig 11. shows the tonal BPF values of baseline and liner configurations. We see that there are 8xBPFs during the testing and the liner is effective and shows a noticeable reduction in SPL at all 8xBPFs.

Further, five aft array microphones 19 to 23 wherein the reduction in SPL was maximum is considered and the dB loss at the 8xBPFs are shown in Fig 12. We see that all five microphones 19 to 23 record significant dB loss with the liner relative to the baseline configuration at all the 8 BPFs. The tonal BPF dB loss and maximum dB loss for respective shaft orders, as recorded by corresponding aft microphones (between 19 to 23), are listed in Table 1. In this result case, the shaft order can also be expressed in terms of fan blades i.e., shaft order = Freq/16 (# of fan blades).

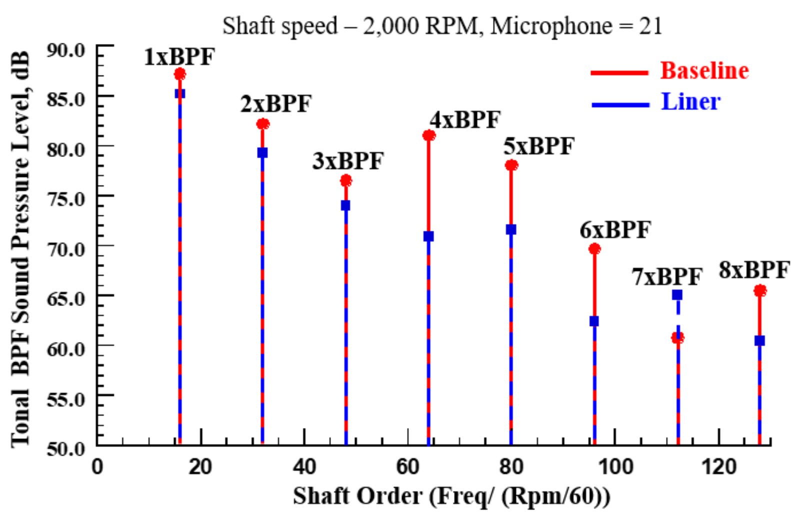

Fig 11. Tonal Blade Passing Frequency SPL for baseline and liner configurations

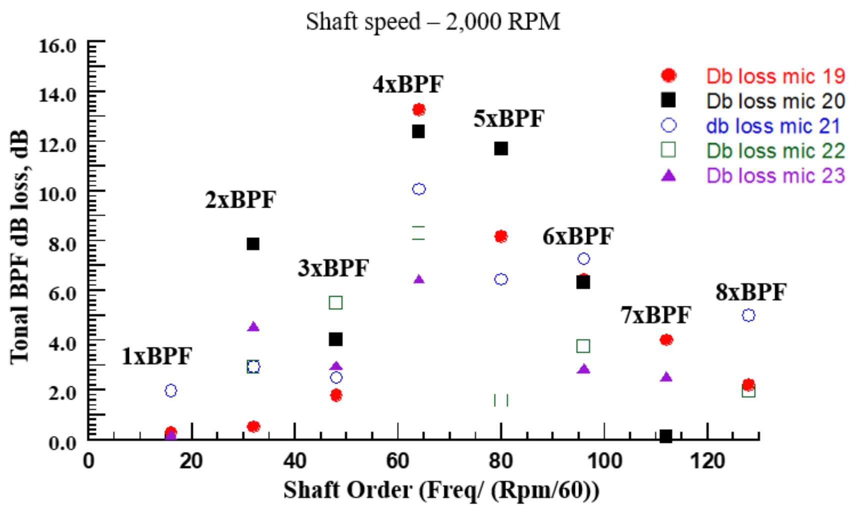

Fig. 12 Tonal Blade Passing Frequency dB loss of 19 to 23 aft array microphones

Table 1: Tonal BPF dB loss recorded by aft microphones 19 to 23 for different shaft orders

Shaft Order	dB loss, dB	Maximum dB loss, dB	Microphone
16 (1xBPF)	0.2 to 2	2	21
32 (2xBPF)	0.4 to 8	8	20
48 (3xBPF)	2 to 5.5	5.5	22
64 (4xBPF)	6 to 13	13	19
80 (5xBPF)	1.5 to 12	12	20
96 (6xBPF)	3 to 7	7	21
112 (7xBPF)	0.2 to 4	4	19
128 (8xBPF)	2 to 5	5	21

2. Broadband sound pressure level response

In the case of broadband response, the data are in the form of signals, so these measurements need to be smoothened to eliminate the noise and analyze the data. The raw broadband response of SPL versus shaft order for baseline and liner configurations for microphone 21 for 2,000 RPM shown in Fig 13 requires smoothening.

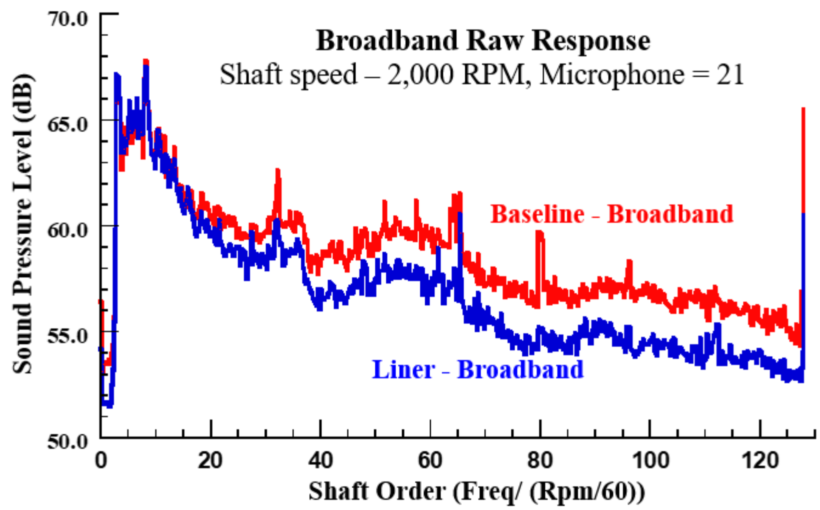

Fig 13. Raw broadband SPL versus shaft order for baseline and liner configurations

As mentioned there is a need to smoothen the data to analyze and interpret the results. Hence the measured data were smoothened using a robust locally weighted regression (rLowess) method [12] in MATLAB. This rLowess method that was applied to the fatigue model for data reduction [13] is adapted here.

Fig 14 shows the smoothened broadband response of SPL versus shaft order for baseline and liner configurations. From the results, we see that the liner configuration reduces the noise level beyond the shaft order of 20 and the reduction in noise level increases with the shaft order. The dB loss ($SPL_{baseline} - SPL_{liner}$) is noticeable beyond shaft order 20, increases with the shaft order, and varies between 2 to 3 dB beyond shaft order 40.

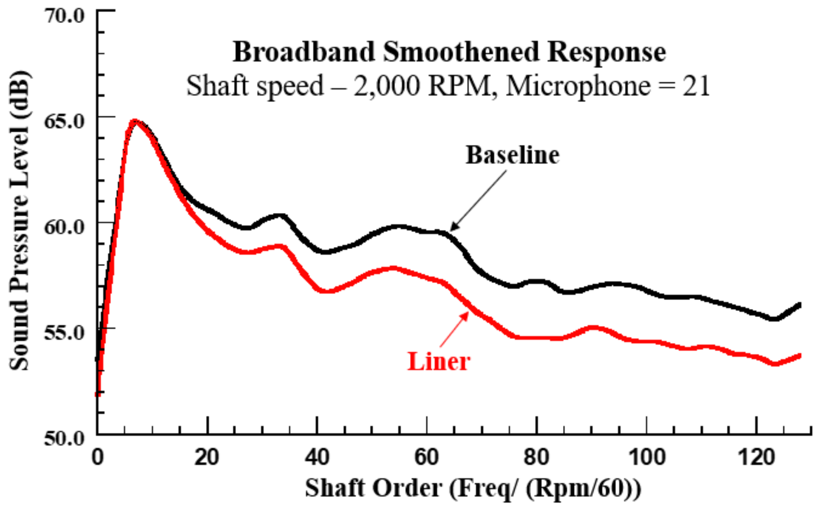

Fig 14. Smoothened broadband SPL versus shaft order for baseline and liner configurations

A dB loss for a broadband response versus shaft order ($\text{Frequency}/(\frac{\text{RPM}}{60})$) between the baseline and the liner configurations is as shown in Fig. 15 for a typical region of 105 to 160 deg (microphones 19, 20, 21, 22 and 23 respectively are plotted) was analyzed. From the result, we see that for a shaft order of 20 (667 Hz) the dB loss is > 1 dB and increases with a further increase in the shaft order with a maximum dB loss of 2.70 dB. Also, the maximum dB loss was recorded in the region of microphones 19 to 23 (highlighted in Fig. 8). Further, co-relating this ANCF test liner result to impedance test results (See Fig. 1 and 2), the acoustic liner is effective beyond 600 Hz. Based on this test result, we can design (control microstructure) the acoustic liner by optimizing the particle size, distribution through the thickness, layer thickness, and total thickness to improve the dB loss. The present results are for a 2-layer in 50 mm thick liner. This paper demonstrated the idea that a passive system of 3D micro-structure controlled graded porous media can be used to mitigate the noise. The dB loss can be further enhanced by optimizing the design.

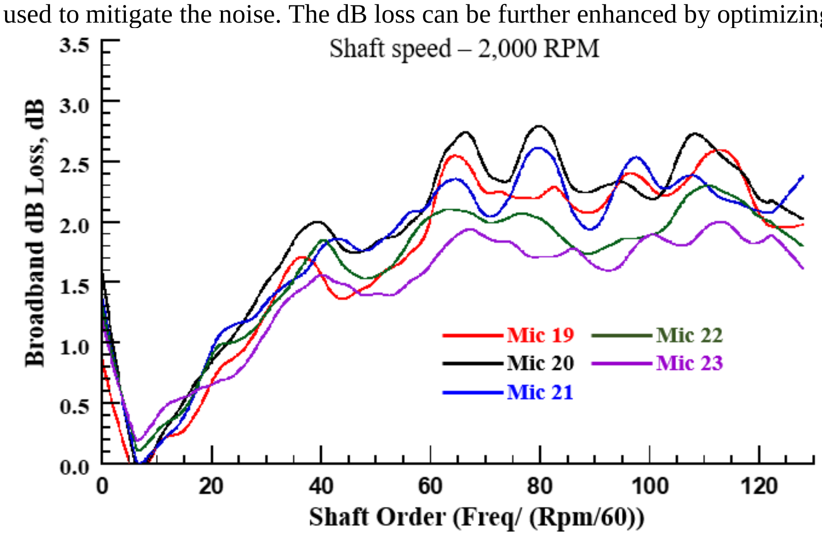

Fig 15. Broadband dB loss versus shaft order of aft microphones 19, 20, 21, 22, and 23 between baseline and liner configurations.

C. Effect of turbomachine shaft speed on dB loss

In this study, the tests were conducted at 5 different turbomachine shaft speeds of 1,500, 1,600, 1,700, 1,800, 1,900, and 2,000 RPM. The tonal and broadband responses are analyzed and discussed separately.

1. Tonal Blade Passing Frequency dB loss response

As mentioned, tonal noise constitutes the major part of the overall fan noise, especially the BPF noise which is generally the most dominant component. Figure 16 shows the tonal BPF dB loss versus shaft order of microphone 21 for 8xBPFs for turbomachine shaft speeds of 1,500 to 2,000 RPM with increments of 100 RPM. We see that the dB loss is different at different shaft speeds for all 8xBPFs, but the liner is effective in all cases for microphone 21. Similarly, we noticed that the liner was effective as per the recorded noise levels of microphones 19 to 23 (a highlighted region in Fig 8).

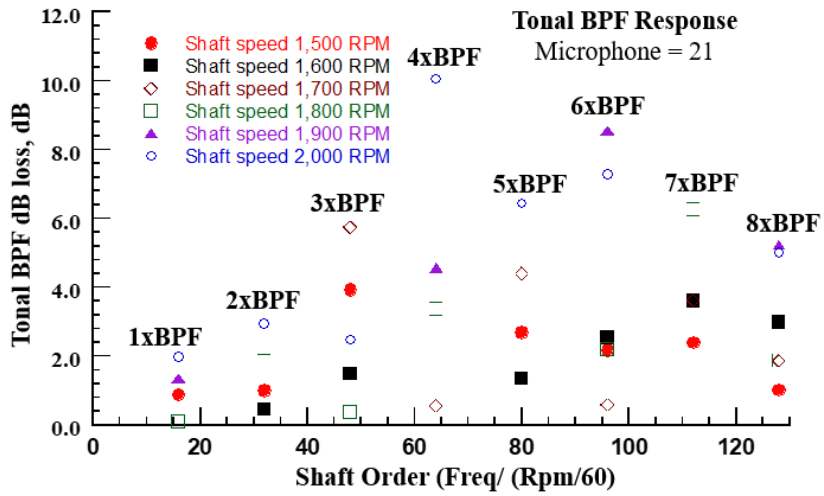

Fig 16. Tonal BPF dB loss of microphone 21 at shaft speeds of 1,500 to 2,000 RPM.

2. Broadband dB loss response

The broadband dB loss for microphone 21 at different shaft speeds of 1,500 to 2,000 RPM is shown in Fig 17. From the results, we see that for the shaft order 40 and beyond, for all the shaft speed cases the dB loss is at least 1.5 dB and increases with an increase in the shaft order varying between 2 to 3 dB. From this, we can conclude that the liner shows similar dB loss as recorded by microphone 21 at all the tested shaft speeds. Similarly, we noticed that the liner was effective as per the recorded noise levels of microphones 19 to 23 (the highlighted region in Fig 8).

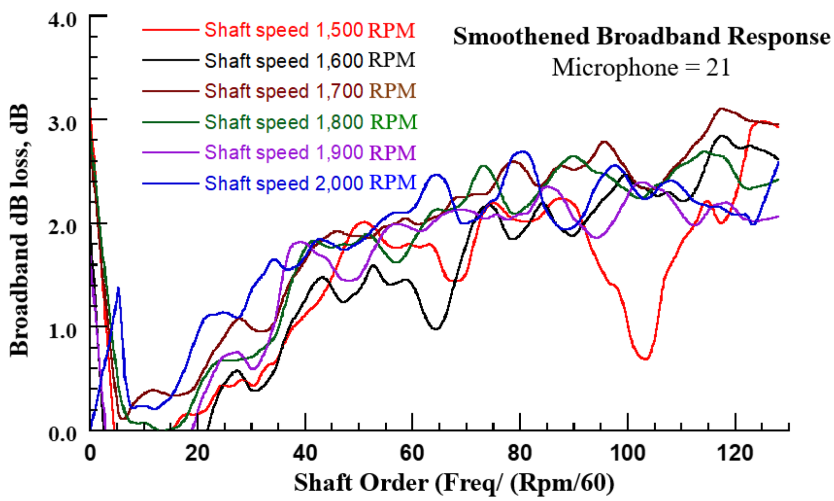

Fig 17. Broadband dB loss of microphone 21 at shaft speeds of 1,500 to 2,000 RPM.

IX. Concluding Remarks

Eight segments of 45º each two-layer acoustic liner of a total thickness of 50 mm with each layer of 25 mm thickness; the innermost layer is made of large size particles of the mean particle diameter of 625 µm and the outer layer is made of medium size particles of the mean particle diameter of 160 µm was fabricated to validate the microstructurally controlled multilayer material for a real ANCF engine. The liner was assembled and tested on an ANCF engine at a University of Notre Dame facility. The test conditions involved acquiring far-field acoustics data for baseline and liner configurations. Far-field acoustic measurements were acquired using 30 microphones placed at a 12-foot radius from the duct centerline and 10 feet high. Fifteen (1-15) of these were in an arc about the inlet exit plane (0° - 90° measured from the inlet axis, Fwd array) and Fifteen (16-30) were in an arc about the exhaust exit plane (90°–160° Aft array with 180° being the exhaust axis). The tone and broadband SPL response data points were extracted separately by running MATLAB scripts.

The assessment of the impact of the proposed concept led to specific conclusions.

- Fwd array microphones at the inlet exit plane recorded insignificant or no difference in SPLs between baseline and liner and this is expected as the microphone locations are at the inlet ahead of the liner setup.
- Aft array microphones 19 to 23 placed at an angle of 105 deg to 125 deg at the exhaust recorded the maximum reduction in SPLs for shaft speeds of 1,500 to 2,000 Hz.
- The current liner design is effective and showed noise reduction of about 2 to 13 dB for tonal noise and about 2 to 3 dB for the broadband noise

The present work demonstrated that a 3D microstructurally controlled graded porous material aircraft liner can be built and effectively reduce the noise of an ANCF engine.

Acknowledgments

The authors thank the support of Dr. Mark H. Ross, Dr. Mike, Mr. Kelvin, Mr. Owen, and Prof. Scott Morrison, University of Notre Dame Turbomachinery Lab for conducting the acoustic liner testing and providing the test data.

The last two authors also thank NASA Glenn Research Center for providing the ANCF test rig engine to conduct the liner test. This work was supported by the NASA Advanced Aircraft Transport Technology Project/ Power and Propulsion sub-Project under contract # 80NSSC21P0133

References

[1] Kenchappa, B., "Development of Lightweight Multifunctional Porous Material for Aircraft Noise Mitigation," North Carolina Agricultural and Technical State University ProQuest Dissertations Publishing, 29067090, 2022.

[2] Berardi U., Iannace G., "Acoustic Characterization of Natural Fibers for Sound Absorption Applications," *Building and Environment*, Vol. 94, No. 2, 2015, pp. 840-852. doi:10.1016/j.buildenv.2015.05.029

[3] X. Xinzhao X., Guoming L, Dongyan L., Guoxin S., Rui Y., "Electrically Conductive Graphene-Coated Polyurethane Foam and its Epoxy Composites," *Composites Communications*, Vol. 7, 2018, pp. 1-6. doi: 10.1016/j.coco.2017.11.003

[4] Crocker M.J. and Arenas J.P., *Use of Sound-Absorbing Materials*, Handbook of Noise and Vibration Control, Wiley, New York, 2007, pp. 696–713.

[5] Arenas J. P., and Crocker M. J., "Recent Trends in Porous Sound-Absorbing Materials," *Sound & Vibration,* Vol. 44, No. 7, 2010, pp. 12-18.

[6] Kenchappa, B., Shivakumar, K., "Development of Lightweight Micro-Porous Materials for Acoustic Applications," *Journal of Composite Materials*, Vol. 56, No. 29, 2022, pp. 4433-4447. doi: 10.1177/00219983221134151

[7] Daniel L. Sutliff., "A 20-Year Retrospective of The Advanced Noise Control Fan," *Contributions to Aeroacoustics Research*, NASA/SP, 2019, URL: https://ntrs.nasa.gov/api/citations/20190030361/downloads/20190030361.pdf

[8] Kelvin M. Figueroa-Ibrahim., Scott Morris., Mark Ross., and Daniel L. Sutliff., "Evaluation of Radiated Sound from the Advanced Noise Control Fan Facility in an Outdoor Environment Using Ground Microphones", *AIAA,* 2019, 3825. doi: 10.2514/6.2019-3825

[9] ASTM E1050–12, "Standard Test Method for Impedance and Absorption of Acoustical Materials Using a Tube, Two Microphones, and a Digital Frequency Analysis System", *American Society for Testing and Materials*, New York, 2012.

[10] ASTM E2611–09, "Standard Test Method for Measurement of Normal Incidence Sound Transmission of Acoustical Materials Based on the Transfer Matrix Method", A*merican Society for Testing and Materials*, New York, 2009.

[11] Joseph McAllister., Raymond A. Loew., Joel T. Lauer., and Daniel L. Sutliff., "The Advanced Noise Control Fan Baseline Measurements," *AIAA*, 2009, 0624, URL: https://ntrs.nasa.gov/api/citations/20090042749/downloads/20090042749.pdf

[12] MathWorks: Filtering and Smoothing Data, [Online Available], URL: https://www.mathworks.com/help/curvefit/smoothing-data.html#bq_6ys3-8 [retrieved 13 February 2022].

[13] Shivakumar K. N., "Total Fatigue Life Modeling and Data Reduction Methods," *AIAA/ASCE/AHS/ASC Structures, Structural Dynamics, and Materials Conference*, 2018.